

Low-current Scanning Tunneling Microscope for Nanoscale Imaging

R.K. Kale

Defence Institute of Advanced Technology, Pune-411 025

ABSTRACT

Advances in the nanotechnology, which is still in its infancy, will depend on our ability to design, build, replicate, and mass-produce usable nanoscale systems. At sub-nanometer length scales, scanning tunneling microscopy (STM) and the related techniques, collectively called scanning probe microscopies, replace the optical microscopy for real-space imaging and manipulation of materials. STM operation is based on measurement of current due to tunneling of electrons across a finite potential barrier between the probe and the sample. In conventional STM, tunneling current of tens of nA and probe-sample distance of a few Å are maintained. These conditions, while necessary for atomic-scale imaging under ultra high vacuum environment, are not suited to handle nanostructures. Quantum structures deposited on a flat substrate usually present a non-metallic sample, and the roughness levels involved are much too high for conventional STM. STM operation with low tunneling current (few pA) and larger tunneling gap (several nm) is preferred to overcome these difficulties. This paper presents experimental work and theoretical considerations for developing an atmospheric low-current STM (LC-STM). Researchers from diverse fields can build their own LC-STM for routine imaging and spectroscopy. Several design details are included keeping this aspect in mind.

Keywords: Nanoscale imaging, low-current STM, nanotechnology, scanning tunneling microscopy, scanning probe microscopy

NOMENCLATURE

		$\Delta s=(s_2-s_1)$	Width of the tunneling barrier
I	Tunneling current	k	Boltzmann constant
V	Tip-sample bias voltage, sample being positive	T	Absolute temperature
s	Tip-sample distance	ψ	Wave function of tunneling electron
$V(x)$	A generalised potential function with sloping sides, representing overlap of tip and sample wave functions. Distance x is measured axially across the tunnel junction	\hbar	$h/2\pi$, h being Planck's constant
s_1, s_2	Points along x where $e \times V(x)$, on its two, opposite sloping sides, equals tip Fermi energy level	m	Mass of electron
		J	Tunneling current density
		$E(x)$	Electron energy at x
		$\phi(x)$	Barrier height at x

$\bar{\phi}$	Average barrier height	$\frac{1}{\Delta s} \int_{s_1}^{s_2} \phi(x) dx$
ϕ_0	Height of ideal rectangular barrier between tip and sample	

1. INTRODUCTION

Basic nano materials research involves structures having at least one dimension of about one to a hundred nm. In nanometer-sized particles with negligible scattering losses, sharp quantisation of electron energy occurs along the length/s that is/are few times the de Broglie wavelength producing quantum well, wire or dot. If the scattering is purely elastic, quantum coherence of the electron motion is not destroyed even for distances exceeding the mean free path. This makes it possible to use quantum dots, for example, as the building blocks of nanoscale electronic circuits. Single-walled carbon nano tubes (CNT) are prospective components of nanoscale electronic devices and field effect transistors (FETs) have been successfully fabricated from these¹. A material with desired properties can be designed using quantum dots as macro atoms² by assembling these into a crystal structure after capping with carefully chosen organic molecules available in wide range of lengths and chemical properties, that become interconnects in the designed solid.

Conventionally, there is a range of imaging techniques and indirect methods to characterise materials at nano and sub-nano scales. Conventional imaging techniques project the periodic structure of a solid (bulk or surface) as the reciprocal lattice suppressing the crucial surface defects and composition. To the extent of real-space imaging of nanoparticles, the transmission electron microscope (TEM) is often used to produce just shadows. No conventional technique could be used as a tool for, say, cutting and locating pieces of CNT. Invention of STM³ first provided a way to image and then physically interact with the systems at nanometer scale. Whereas the STM in its original form was aimed at atomic-scale imaging and spectroscopy, it has become a valuable tool for research on nanoscale systems. Working principle of the conventional STM is straight forward⁴. A piece of metallic wire sharpened at the end down to a small cluster of atoms (tip) is brought

within a few Å of a sample where the wave functions of the tip and the sample electrons overlap to produce a narrow potential barrier of height, the order of their work function. The sample is then biased with a few mV dc voltage which lowers its work function wrt that of the tip allowing tip electrons near the Fermi level to tunnel through the barrier to the sample if vacant states exist (as in the case of metallic sample). This tunneling current has inverse-exponential dependence on the tip-sample distance, which combined with precise control of tip-sample distance, is the key to unprecedented atomic resolution of STM.

The tip is attached to a piezoelectric actuator for precise 3-D motion in the vicinity of the sample. Under constant current operation, a servo maintains the tunneling current constant while the tip is scanned over the sample surface in a raster pattern by synchronised ramp (X) and step (Y) voltages from a computer. Numerical values of X, Y and the correction signal produced by feedback electronics (to maintain the current constant) are saved as three data files in the computer to plot and process 3-D map (image) of the sample surface with atomic resolution. Theoretically, the tunneling current measures the density of states (DOS) at the tip location. Therefore the conductance plot (I–V relationship of the tunneling junction) reflects energy band structure at that location of the sample with resolution few times the thermal energy $k_B T$. This is tunneling spectroscopy and adds to the power of STM. For known energy distribution of the tip, the normalised conductivity, $(dI/dV)/(I/V)$, gives the local density of state (DOS) of the sample without significant distance dependence⁶.

As for the nanoscale materials such as CNT and nanoparticles, these are often deposited on a flat, metallic or graphite substrate for study with a STM. Image interpretation under such conditions requires a fair knowledge of the tip, substrate, and relevant imaging mechanism.

1.1 Low-current Operation

The conventional STM employs a tip bias, that is a small fraction of metalwork function and tunneling current of tens of nA; conditions suitable for good

conductivity samples. When nanostructures (eg nanoparticles, soft biological molecules) are present on an atomically flat substrate, the close ($< \text{nm}$) proximity of tip and sample can displace or damage the sample material due to unwanted tip-sample interactions. Withdrawing the tip from the sample drastically reduces the tunneling current and feedback control is easily lost. Such samples and other low conductivity samples require low-current operation combined with bias voltage exceeding tip work function. With a view to apply the STM technique to samples having low conductivity and high roughness levels, feasibility study of a LC-STM was undertaken using some makeshift hardware, and stable operation down to 87 pA tunnel current over wide range of bias voltage was achieved⁷. This work, which reported successful imaging of boron-doped CVD diamond was followed up by building an all new LC-STM unit with better material (eg aluminum was used for STM head as against perspex sheet used in the earlier work), improved hardware design, novel tip preparation technique, and high performance electronics.

Overall performance of this new LC-STM is an order of magnitude better than the version tested for feasibility. Stable imaging of a variety of samples under tunneling current of a few pA and over wide bias voltage range has become possible. Design,

analysis, and experimental details of this LC-STM have been taken up in this paper. Low-current high-bias voltage operation brings in other tunneling mechanisms, eg near-field emission and field emission, which qualitatively differ from the normal metal-vacuum-metal (MVM) tunneling. This calls for clear understanding of the imaging mechanisms and caution in image interpretation. Thus, a theoretical picture of these aspects is also included.

2. CONSTRUCTION AND EXPERIMENTAL DETAILS

At the heart of the LC-STM is the STM head consisting of scanner, tip, sample, approach mechanism, a low-current preamplifier, filter, and an instrumentation amplifier. This, along with an electrostatic-cum-acoustic shield, is supported on a vibration isolation platform. Scanner electronics and computer are interfaced with the STM through a junction box, from where all connections to the STM are made using 48 SWG enameled copper wires which carry electrical signals with negligible mechanical disturbance.

2.1 Scanning Tunneling Microscopy Head

The geometrical details of the STM head built in aluminum are given at Fig. 1. The bottom structure forms a channel on one side and a recess (IA, PS)

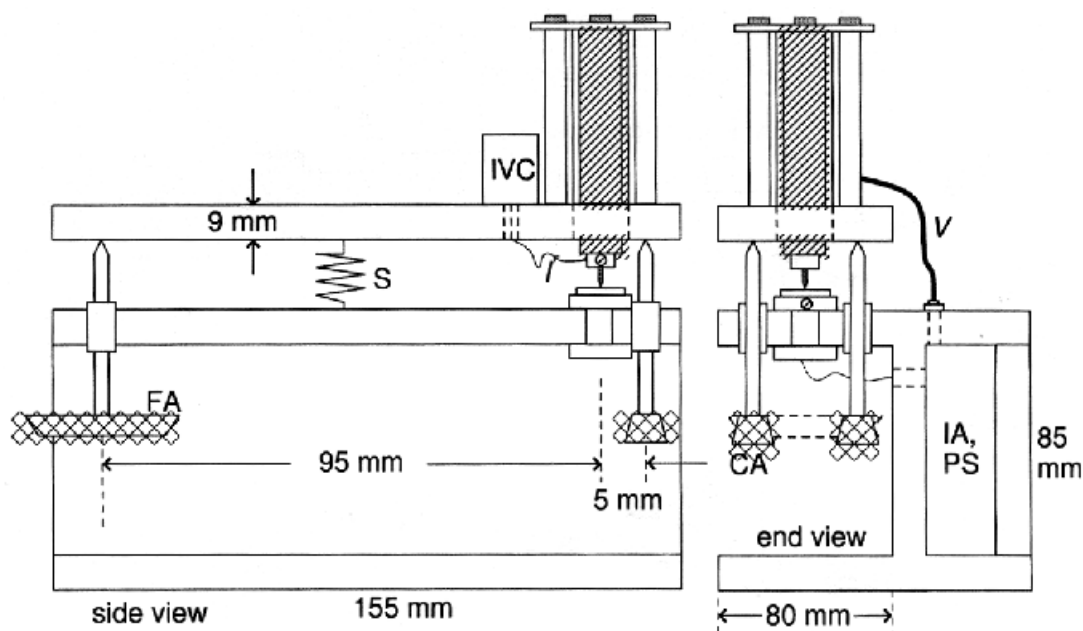


Figure 1. Dimensional sketch of the STM head built with aluminum plates fastened together.

for housing low-current electronics and battery pack on the other side. The top plate is supported on three pointed screws and is held in place by a drawing board clip, shown symbolically as a spring. This plate, carrying the piezo scanner, is removed for installing the tip. I indicates current input to the I/V converter whose output is led to the recess, (IA, PS). The lower part is constructed with 10 mm rectangular plates fastened together to provide a 155 mm long channel on one side and a recess with a cover to house instrumentation amplifier and batteries on the other side. This can be seen in the side view showing cross section of the part. Fasteners are not shown in the figure. The top plate of the channel has two screws at one end (aligned perpendicular to the channel) and one screw at the other. Together, as seen from the top, these form an isosceles triangle of 100 mm height. Within this triangle and 5 mm away from its base is located, symmetrically, the centre of the sample holder, which is similar to a SEM sample holder.

As seen in the side view, the sample holder is located within the triangle, 95 mm from the single end-screw and 5 mm from the pair of screws on the other end of the channel. On this copper sample holder, a 1 cm² sized sample can be held by a spring (for top contact) or by silver paste (for contact at its bottom). On the triangle formed by three pointed screws is supported a single rectangular plate carrying the piezo scanner. Due to the lever action, as the end screw is lowered by h keeping the pair of screws on the other end fixed, the tip moves only $0.05 h$. The pair of screws on the right in the figure provides coarse positioning of the tip while the lone screw on the left in the figure, which has fine (70 tpi) threads provides fine positioning. Movement of fine control screw is improved by providing a large dial (dia 6 cm) for fine adjustment at its lower end, FA in the figure. Together with this dial, manual tip motion sensitivity of $0.1 \mu\text{m/mm}$ of tangential motion of the dial is achieved. The sample holder is push-fitted into a metallic base having a tubular hole above and passing through the aluminum plate below to provide a solderable contact terminal. The metallic base itself is insulated from the aluminum plate by a ceramic stand off.

2.2 Piezo Scanner Mounting

A 25.4 mm long tubular piezo with inner dia of 6.35 mm, wall thickness of 0.55 mm, and resonant frequency of 40 kHz from the previous work⁷ was used. It was mounted on the top plate of the STM head (Fig. 1) as follows. One end of the piezo was carefully adhered with a thin layer of adhesive by brand name Araldite to a circular disc, with a hole in the centre, made out of machineable ceramic. This disc also had four, symmetric, peripheral holes for mounting. Four long screws, as shown in Fig. 1, were used to fasten the piezo-carrying disc through the shell with top plate such that the free end of the piezo looked down at the sample through a hole at the aluminum plate. To the free end of the piezo was similarly adhered a small tip holder made of copper to hold thin metallic tip with threaded screw. X and Y tip motions were achieved by applying voltage to the outer four quadrants whereas the Z motion was controlled by the voltage applied to inner wall of the piezo. The horizontal and vertical sensitivities of the piezo were 100 \AA/V and 50 \AA/V , respectively. Terminals were provided on the top surface of the piezo holder disc for connections and voltage signals to these terminals were carried on thin, 48 SWG copper wires.

2.3 Low-current Electronics

The essential low-current electronic circuits completely replacing those in the earlier version⁷ are shown in Fig. 2. Referring to this figure, sample bias of desired polarity was generated by unit (a) with a ten-turn helical potentiometer and a polarity selector switch. This unit was installed outside the STM body at the junction box which interfaces the STM body with other systems. Bias voltage and an ac signal (if used for lock-in application) were carried to the STM body by thin 48 SWG wires. These were connected to input of the adder at (b), which was installed in the recess IA, PS in the STM head (Fig. 1). Output of the adder was connected to the base of the sample holder by passing a sturdy wire through a hole in the aluminum wall. Tunnel current was collected from a soldered connection at the tip holder as shown in Fig. 1 by a very short wire which enters through a hole on the top plate

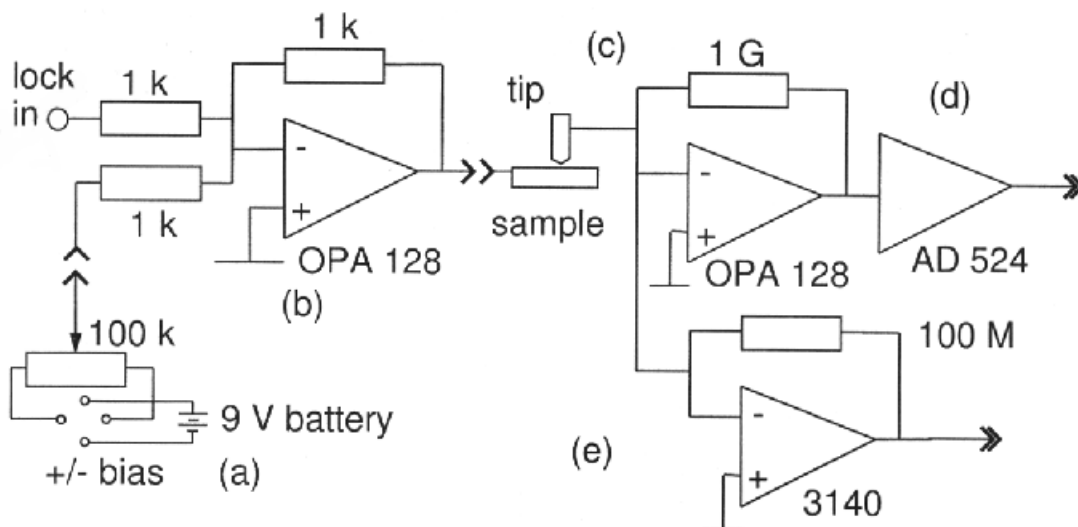


Figure 2. LC-STM preamplifier and the associated electronics: (a) sample bias control, 0 to $\pm 9\text{V}$, installed at the junction box outside the STM, (b) adder-cum-isolator IC employed to connect sample bias and, optionally, to add a small ac signal to sample bias for lock-in applications, (c) low-current I/V converter, (d) instrumentation amplifier with switchable gain settings (not shown), and (e) alternate I/V converter for normal STM operation.

into a small aluminum box housing I/V converter, installed next to the piezo. This I/V converter is shown as (c) in Fig. 2. This is a crucial unit. Voltage output of the converter enters the IA, PS recess of the STM head through a coaxial connector. Inside the recess is installed the instrumentation amplifier (d) along with the other I/V converter (e). The recess also houses a battery pack of four 9 V dry batteries interconnected with a DPDT switch (on the cover plate) with 10 k pF DC capacitors to suppress ringing. This battery pack provides the $\pm 18\text{ V}$ op-amp supply to all the electronics on the STM head. Instrumentation amplifier has selectable gains of 10/100/1000 to give an output of 1 V/nA to 1 V/pA. As the feedback controller accepts a maximum of 1 V, this puts an upper limit of 1 nA on the tunneling current in STM operation. Therefore, as an option for normal STM operation in the tunnel, current range 1-10 nA, another I/V converter (e) in Fig. 2, was provided. Output of the instrumentation amplifier (or of the optional I/V converter) was carried, again on thin wires to the junction box outside the STM. The STM head, as also the vibration isolation platform and shielding cover, were grounded to an earth conductor made to IS standards.

2.4 Scanning Electronics

Synchronised step and ramp voltages were applied to the tubular piezo to scan the tip over the sample. These signals were produced by computer with an available C program through a PCL 208 AD/DA card from Dinalog. To improve the performance and scanning range over the earlier version⁷, a new, rugged interface unit was built using simple op-amp circuits in IC 3140. It performed the following tasks in the stated order:

- Shifting of 0–5 V D/A converter output to $\pm 2.5\text{ V}$, amplifying it to $\pm 5\text{ V}$ and then providing an overall dc shift of $\pm 5\text{ V}$ to both signals.

Thus scanning signal corresponding to $\pm 5\text{ V}$ can be shifted by another $\pm 5\text{ V}$. When applied to the HV direct-coupled amplifiers⁷ with gain 20, scanning voltages (ramp to X and step to Z piezo section) of $\pm 100\text{ V}$ were available with dc offset of another $\pm 100\text{ V}$ from zero. Recalling that the piezo has a lateral sensitivity of 100 \AA/V , The net result is that sample can be scanned and images recorded over a range of $2000 \times 2000\text{ \AA}$ area with six overlapping sections of $1000 \times 1000\text{ \AA}$ each, without having to disturb the feedback loop. This is best illustrated in the STM images given at

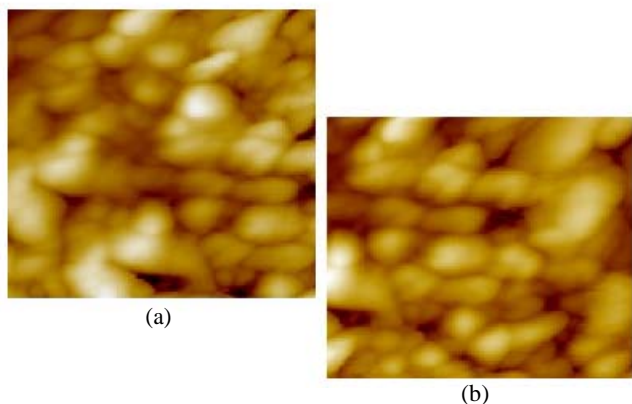


Figure 3. (a) Gray scale, low current, $940 \times 940 \text{ \AA}$ size images of capped silver nanoparticles deposited on gold surface (b) the second image was obtained after applying a dc offset to the piezo, to image an adjacent sample area.

Fig. 3, where images taken with different locations of equilibrium position of tip are placed together. The common features can be readily identified. It may be noted that the images are raw, without any filtering or other processing. An oscilloscope is used to adjust dc offsets.

2.5 Signal Linearisation and Feedback Control

The tunneling current with its exponential dependence on tip-sample distance has to be linearised

by a log amplifier before it can be conveniently servoed for constant-current operation. Figure 4 shows the controller design adapted from the previous work⁷. The first two op-amps with two diodes in the circuit ensure negative input to log amplifier regardless of the polarity of instrumentation amplifier output. Log amplifier is wired for $I_{ref} = 10 \mu\text{A}$, so that controller locks at $E_{ref} = R_{in} \times I_{ref}$ where R_{in} is set by VR1. Output of the log amplifier is fed to the integrator which is followed by a gain amplifier. Ten-turn potentiometers are used for precision setting of R_{in} , integrator time constant and proportional gain. Signals can be tapped at various points to test the controller. As shown in the figure, instrumentation amplifier output is applied in unipolar form to the log-amplifier IC, 755P, which has a $10 \mu\text{A}$ current reference I_{ref} . Voltage can be servoed at any value between near-zero to a maximum of 1 V by inputting this $10 \mu\text{A}$ current through a $100 \text{ k} \Omega$ ten-turn potentiometer (note the product of two quantities). Controller itself is proportional-integral (PI) type with adequate manual interface through precision ten-turn potentiometers for setting the controller parameters. The controller box also houses a bank of three high voltage dc coupled amplifiers, each with gain of 20. Output of the feedback controller is applied to one of these and the amplified output is connected to junction box by patch cord, from

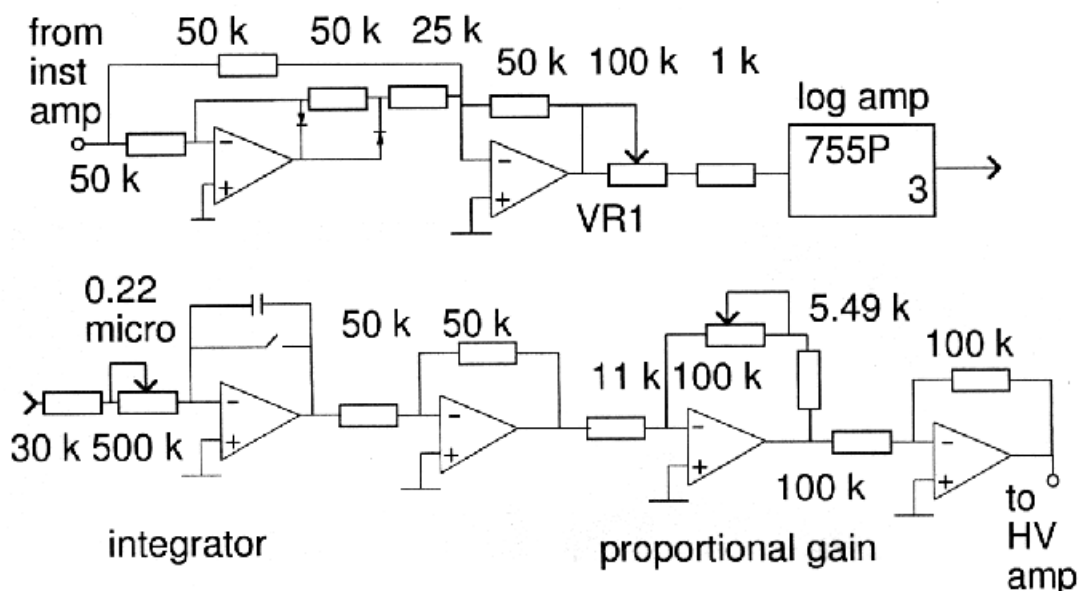


Figure 4. Feedback controller circuit (design from work by DiLella⁸).

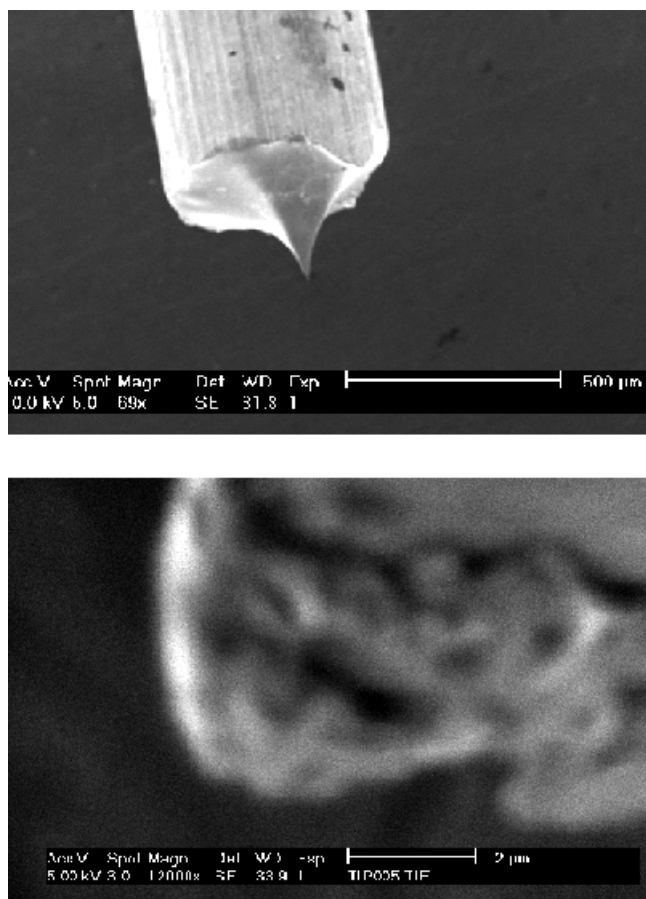


Figure 5. SEM images of a high aspect ratio W tip prepared from 0.38 mm dia, high purity polycrystalline tungsten wire. Image at the top shows fractured surface. Fracture leaves asperities with atomic clusters at the end of the tip, not resolved by SEM. Ideally, only one of these, the nearest to the sample, will contribute to tunnel current.

where it proceeds on thin wire to the Z section of the piezo for tip-sample distance control. The other two HV amplifiers are utilised by the scanning electronics.

2.6 Tip Preparation Technique

The tip preparation technique was considerably improved over the previous work. While the standard method of electrochemical etching⁴ was adapted to prepare tips, a new tip etching unit was built with a manipulator using 70 tpi screw. A tungsten wire was held in a conducting holder and a large dial (5 cm dia) was used for fine control of its vertical motion in and out of an electrochemical

cell containing 1 N aqueous solution of *NaOH*. High aspect ratio tip, as shown in Fig. 5, was obtained with a novel approach as follows. The W wire piece to be etched was covered with two sharply cut pieces of PVC sleeves (from a multi-strands wire) at the end with a small gap between these. This end was lowered into the electrochemical cell such that a liquid meniscus filled the gap between the sleeves where tungsten surface was exposed. A bias of 12 V dc was applied to the cell with the tip positive. Within minutes, the electrolyte etched away the material between the sleeves. As the lower part dropped off, the meniscus disappeared and liquid level dropped below the etched end ensuring that tip did not become blunt due to continuing liquid contact.

2.7 Vibration and Acoustic Isolation

STM head needs to be isolated from electromagnetic interference (EMI), building vibrations and acoustic disturbances. A commonly used arrangement involves suspending the STM head with long, well designed springs in an enclosure, well protected from other disturbances. Instead, a simple table-top arrangement, well-improvised over the previous version⁷, was used for the LC-STM. To this end, five numbers of square, highly polished steel plates with gradually decreasing size were manufactured and piled up in a stack, width decreasing top-down, to provide a platform to place the STM head. These plates were separated by randomly oriented small pieces of rubber tubings commonly used in the bicycle tube valve. This stack was placed on two iron rounds (one 10 mm thick with dia 353 mm and another 20 mm thick with dia 500 mm, together weighing 32 kg) placed one over the other with a soft rubber spacer. Both the plates were thoroughly cleaned and powder coated to maintain a reasonably clean environment. The whole assembly was positioned on a well-inflated rubber tube from a car wheel, which in turn was placed on a heavy table top. This arrangement provided the desired vibration isolation.

To provide static protection, a cylindrical aluminum vessel was used, and aluminum handles at its rim were inverted. When this 25.4 cm tall vessel, open

end down, was lowered over the entire STM assembly, its circular rim of 406 mm dia snugly sat over the outer round plate of dia 500 mm and covered the entire assembly. The rim of the shield was lined with a length of rubber tubing (again, the one used for bicycle tube valve) with a quick drying adhesive to provide soft landing of the shield on the plate. This also protected the 48 SWG wires carrying electrical signals to and from the STM which were taped down on the outer plate. Shield as well as the plates was electrically grounded to the dedicated ground point made to IS standards. On the inside surfaces, this lid (or shield) was well-cushioned using soft material (thermocool) for acoustic protection and blackened for photon emission studies. While the LC-STM worked well with nanoscale sampled in the working hours where considerable building vibrations and acoustic noise existed, the best results were obtained late in the night. An airconditioner running in the laboratory did not make any adverse effect on the performance. The system also showed good EMI protection against emissions from any electrical circuits in the laboratory.

2.8 Design Considerations and Diagnostic Experiments

It is necessary to test the STM for health and reliability of various pieces of the hardware. Beginning with some important design aspects, a discussion on the diagnostic tests will be presented. It is worthwhile to take an objective look at the expected performance at this stage. The STM does not work in UHV environment, and therefore, atomic resolution on the nanoscale samples, or rather the contaminants sitting on them, is not expected. As such, the tip positional accuracy of 0.01 Å as in an atomic-resolution STM, was not crucial to this work. Further, since this equipment worked on the same general principles as applicable to the earlier one assembled for the feasibility study, and only the hardware was improvised for higher reliability and scope, the data on junction characterisation from the earlier work was directly applicable to this version.

2.8.1 *Sample Biasing and Tunnel Current Detection*

In the earlier feasibility version, the bias voltage to the sample was carried on a long, noisy wire. This time, the bias was buffered with a high performance op-amp that also served as an adder. This, with the noise current of $0.2 \text{ fA}/\sqrt{\text{Hz}}$ in the frequency range 0.1 Hz-20 kHz for the op-amp OPA 128 ensured that the noise in the bias never exceeded 0.03 pA. As against the earlier version, the I/V converter was also built with the electrometer grade IC OPA 128 and positioned very close to the tunnel junction. Just 3 cm long flexible 48 SWG wire carried the tunnel current to the op-amp wired with 1 GΩ resistor in a thin aluminum box as a shield that was fastened to the grounded aluminum plate. The small piece of PCB that carried the op-amp was thoroughly cleaned with methanol and dried in nitrogen. To avoid any leakage current, soldering the input lead to the PCB was avoided altogether since it had enough mechanical strength for the purpose. Potentiometer for offset null was not necessary.

Output went to the instrumentation amplifier recess on a shielded wire. it was calibrated as a voltage amplifier by temporarily connecting a 9.66 MΩ resistor at the input and mV level dc applied to this resistor in steps to simulate up to $\pm 100 \text{ pA}$ input current in steps of 10 pA. Instrumentation amplifier, AD 524 was also carefully installed with small jumpers (normally used in computers) for gain selection and calibrated.

2.8.2 *Achieving Tunneling and Thermal Drift*

After the sample was cleaned and attached to holder, the plate carrying the piezo was removed, tip was mounted, the plate was replaced and both the tip and the sample were observed with a traveling optical microscope placed on the same table, away from the STM. A multimeter was connected to check the continuity of tip and sample. Using coarse screws, the tip was brought within a mm or so of the sample. Then fine-approach dial (Section 2.1) was manipulated with thumb observing the approach through the traveling microscope. When the tip appeared to have touched the sample but the multimeter

showed no electrical contact, it was clear that the tip was within a micron or so of the sample. Now on, a stepper motor-based approach was essential to bring the tip within tunneling distance and stop the tip before crashing. Stepper motor control, though easy to build using a small stepper motor, eg from computer hard disc drive, was not employed for this work. Simple calculations showed that cantilever approach mechanism (discussed in Section 2.1) provides about 1 μm vertical tip movement per cm of rolling motion of the finger on the fine approach dial. With slight tapping action on the dial and some luck, tip could be brought within the tunneling range and locked in position by switching-on the feedback control unit.

Often on the onset of the feedback control, the piezo extends enough to feel the tunnel current and lock onto it. Sometime replacement of the tip may be necessary. This is followed by manually applying large tip bias cycles so that the large electric fields so produced remove the unstable tip asperities (whiskers) of ill-bounded atoms and the tip end assumes a stable configuration. STM was allowed to run for about half-an-hour to attain all round electrical and thermal stability before scanning could be attempted. Scanner piezo, its ceramic disc base, and sample stand off, are the materials having low thermal expansion of the order of $10 \times 10^{-6}/\text{K}$ at room temperature. Steel has similar thermal expansion property ($12 \times 10^{-6}/\text{K}$), but aluminum ($23.6 \times 10^{-6}/\text{K}$), was chosen for the STM body for manufacture convenience and clean surface. As such, it imposes the ultimate limit on the thermal drift. While no specific thermal drift data was logged, it is clear from the imaging experience such as the two images at Fig. 3 with several minutes' time lapse between these that thermal drift for the STM was within accepted limits.

2.8.3 *Vibration Isolation Diagnostics*

The rigid construction of the STM head in thick aluminum sheets has high resonant frequency and placing it on the vibration isolation platform lent reasonably good shock and vibration immunity to the STM. At the lower end, the vibration-isolated platform showed a resonant frequency of about

2 Hz. This was ascertained by manually disturbing the base plate and observing the oscillatory motion of the rigid STM head by the traveling microscope. For quantitative diagnostic, the active tunnel junction minus the scanning offers a good sensor for vibration detection through fast Fourier transform (FFT) of the tunneling current, provided it can be distinguished from peaks in the FFT plots originating from electrical disturbances. HP 54601B, 100 MHz oscilloscope having FFT measurements as an option was used for these experiments. Several peaks appearing in the FFT plots were eliminated by reorganising the vibration isolation and grounding arrangements. Two peaks at 635 Hz and 8 kHz remained prominent. Adverse effects of these frequencies was avoided by slow scanning rates (typically, one to several minutes per image) used for this work. Imaging software ensures that each current value is averaged over specified number of values, thus further eliminating the random disturbance errors at the cost of imaging speed.

2.8.4 *Tunnel Junction Diagnostics*

This aspect essentially involves understanding the interrelationship of tunnel current, bias voltage, and barrier width in the STM. As the STM was expected to function over a wide range of sample bias voltage exceeding the tip work function, several conductance plots were obtained over a wide range of bias voltage in the feasibility study. These experiments (Fig. 6, upper plot) revealed three regions of tunneling mechanisms. For small bias voltage ($eV \ll 0$), linear voltage dependence characterising ohmic behaviour was observed. This marks the normal STM operation (few mV bias and several nA tunnel current). For intermediate regions, a nonlinearity sets in. For large voltages ($eV \gg 0$), I-V characteristics were dominated by exponential-behavior. These results are similar to those obtained by Young⁹⁻¹⁰, *et al.* Several tunnel current versus relative tip-sample distance plots, that reveal the feature heights in the STM image, as also the plots of sample bias as a function of change in tip-sample distance have been reproduced in Fig. 7. The latter are essentially required for determining the absolute tip-sample distance under the pure-tunneling conditions by fitting theoretical models.

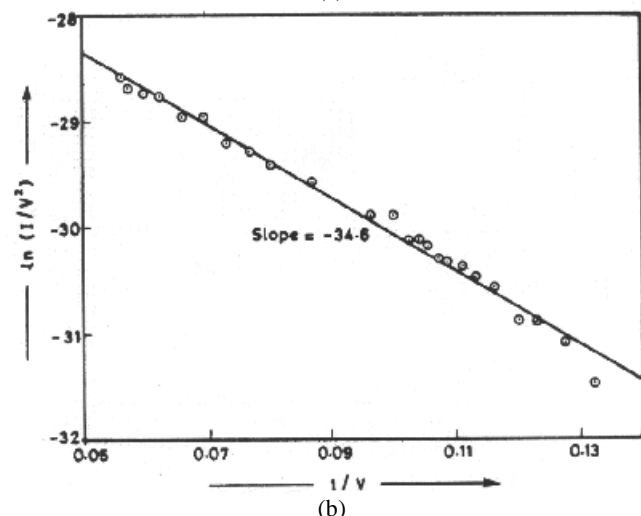
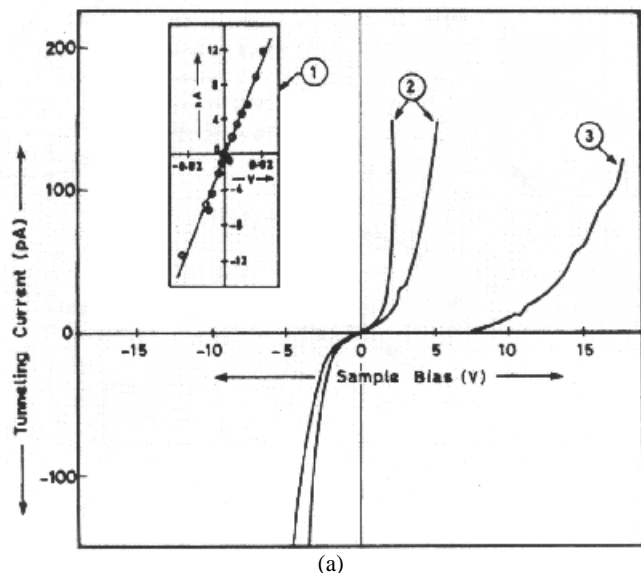


Figure 6. (a) Conductance plots obtained on the STM tunnel junction over a wide range of sample bias voltage with three regimes of tunneling labeled as (1) normal metal-vacuum-metal tunneling with linear I-V relationship, (2) transition region tunneling, and, (3) field emission tunneling. Plots compare well with those obtained by Young^{8,9}, *et al.* and (b) Fowler-Nordheim plot corresponding to conductance plot (3) above, confirming field emission.

2.8.5 Imaging and Image Processing

The size of the scanned images was deduced from the piezo voltages applied to X and Y sections of the scanner piezo combined with its lateral sensitivity of 100 Å/V. The piezo specifications were available from the source and dynamically verified through earlier researchers' work with Michelson interferometry. Similarly, while no absolute height determination

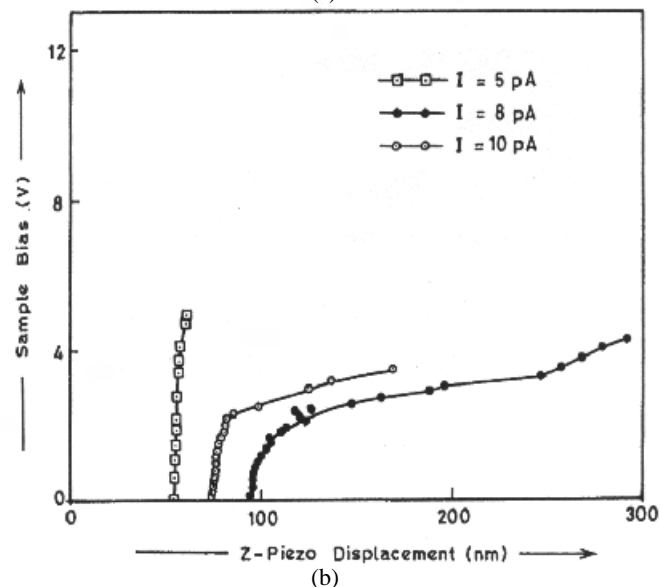
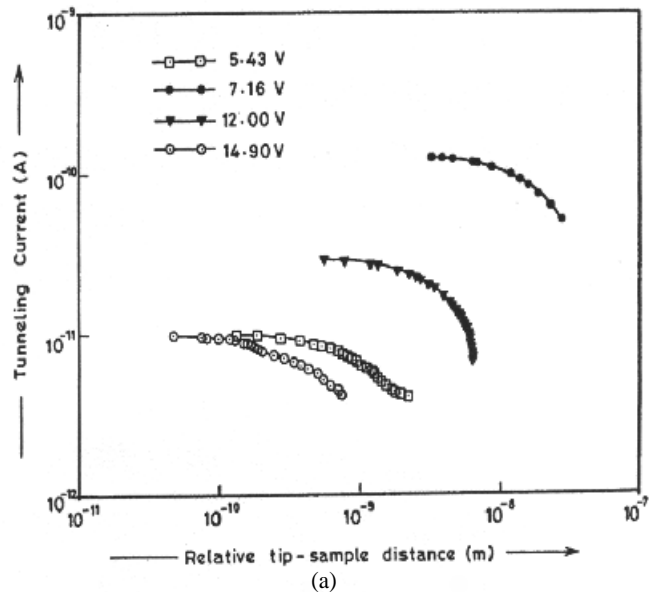


Figure 7. (a) Tunneling current (I) plotted as a function of relative tip-sample distance measured by disconnecting the feedback loop. The four plots covering a wide range of bias voltages are presented on a log-log scale and (b) the three plots show variation of sample bias voltage (V) as a function of relative tip-sample displacement required to maintain constant tunnel currents of 5 pA, 8 pA, and 10 pA. Fitting a theoretical model to these plots would yield the absolute tip-sample distance.

was possible for limitation of theoretical model as well as uncertainties as regards the purity of tip and sample associated with atmospheric operation, relative heights of the image features was deducible from the feedback control voltage signal logged as

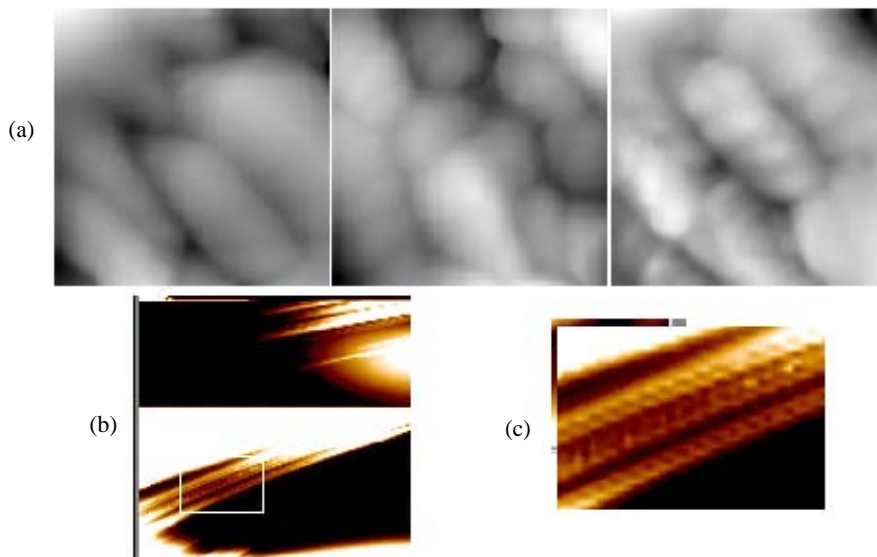


Figure 8. (a) Three gray scale images of size $940 \times 940 \text{ \AA}$ depicting different areas of 1-3 propanedithiol (*PrDT*) deposited on gold substrate. Images were obtained at 5 pA tunneling current and 0.3 V bias, (b) another $940 \times 940 \text{ \AA}$ sized image of PrDT on gold is shown on the left. Horizontal discontinuity is due to z-offset changed midway. The image was obtained at 53 pA, 0.353 V bias, and (c) the inset, software-magnified for clarity, measures $190 \times 128 \text{ \AA}$ and shows horizontal resolution of about 1 nm.

the z variable. However, height specifications have to be viewed in the light of errors arising from operation under atmospheric conditions where impurities can considerably affect the local work function, which in turn affects the tunneling current to produce false corrugations. A free trial version software from SPIP, downloaded from world wide web at imagemet.com/spip was used for constructing images from the data files and performing such operations as tilt correction, noise filtering, histogram equalisation, and line profiling, where required at the bare minimal level. However, all of the images included in this paper are raw images with tilt correction only, but with no filtering performed on these.

3. RESULTS AND DISCUSSION

Four sets of images obtained on the homebuilt low-current STM have been presented here as Figs 3, 8 and 9, the focus being on the imaging capabilities of the LC-STM rather than investigations carried out with the instrument. (Some sample-specific studies have been carried out¹⁰, whose specifics have been briefly stated under the concluding section, viz., Section 4). All the images have been plotted in gray scale. Gray level of a pixel is a measure of relative tip height, not specified except

in Fig. 9, where a line profile depicts the relative tip height along the line on the sample. Figure 3 depicts two $940 \times 940 \text{ \AA}$ sized raw images of silver nanoparticles prepared by γ irradiation of a silver nitrate solution containing organic capping agent. The sample was deposited on gold-coated *Si* substrate. Bias lead was connected to the gold film for imaging. The second image of Fig. 3 was obtained after the equilibrium position of the tip was shifted using dc offset (Section 2.4). Common features can be readily recognised. These and other images of the adjoining area can be combined to get an image of four-time the sample area possible without dc offset.

These images, obtained after several minutes gap in between, also demonstrate thermal stability. Size of the smallest feature size seen in the images indicates the lateral resolution of 5 nm, better than that usually seen in a SEM image. The preceding remark should be seen in the light of the fact that this LC-STM operates under ambient conditions and with a simple table-top vibration-isolation platform. Figure 8 (top three images) again shows absolutely raw images of $940 \times 940 \text{ \AA}$ sized sample area obtained from the surface of gold-coated *Si* substrate on which organic material, *PrDT*, was deposited. The concerned experiment¹⁰ was aimed at depositing

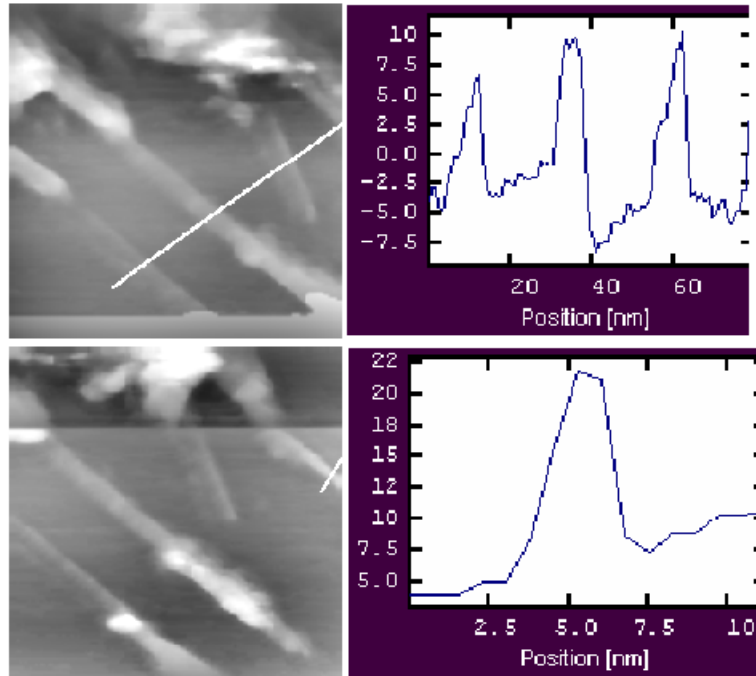


Figure 9. $940 \times 940 \text{ \AA}$ images of CNT deposited on HOPG. Images were obtained at 6.6 pA. The corresponding line profiles show, in units of nm, the relative tip-height variations under constant-current scanning. About 17 nm height variation indicates the capability of the STM to image large corrugations.

a monolayer of *PrDT* to be used as a spacer for depositing *Ag* nanoparticles. The images clearly show randomly sized thick lumps of the material rather than a uniform layer with striking clarity. The gray-scale levels (reference scale not shown) in the images reveal high roughness detectable by LC-STM.

Another attempt to obtain a monolayer on a similar substrate produced altogether different features on the substrate, also shown in Figs 8 (b) and 8(c) (lower left image of size $940 \times 940 \text{ \AA}$ and its blowup measuring $190 \times 128 \text{ \AA}$ on the right). The latter, software magnified section shows a periodic structure of lateral resolution nearly 1 nm apparently revealing molecular arrangement on the substrate. Lastly, Fig. 9 shows low-current images of carbon nanotubes dispersed on a HOPG substrate. Contamination particles are seen sticking to the tubes. The line profile, with vertical scale indicating relative tip height in nm, shows different diameters of the tubes suggesting multi-walled structure.

3.1 Theoretical Considerations

For an insight into the imaging mechanism for nanoscale materials, it is useful to apply the classical theory of tunneling by Simmons¹ to LC-STM tunnel junction. To state the essential results of this theory, a general potential energy barrier of sloping sides between tip and sample was considered. WKB approximation gives the tunneling probability across this barrier as

$$D(E_x) = \exp\left(-\frac{2}{\hbar} \int_{s_1}^{s_2} \sqrt{2m[V(x) - E_x]} dx\right) \quad (1)$$

Current density across the barrier is found out by integration over the available electron energy states weighed by their occupancy probabilities, ie, Fermi functions. Difference of current densities in either directions gives the net current density. Simmons' theory gives

$$J \approx \frac{e}{2\pi\hbar(\Delta s)^2} \left(\bar{\phi} e^{-A\sqrt{\bar{\phi}}} - [\bar{\phi} + eV] e^{-A\sqrt{\bar{\phi} + eV}} \right) \quad (2)$$

where $A = 2\sqrt{2m} \cdot \Delta_s / \hbar$ and V is the tip-sample bias voltage. Three qualitatively different cases of tunneling arise; $eV \approx 0$, $eV < \bar{\phi}$ and $eV \gg \bar{\phi}$. When $eV \approx 0$, Simmons' equation reduces to the case of normal metal-vacuum-metal tunneling characterised by linear I - V relationship. This is normal STM operation. On the other extreme, when $eV \gg \bar{\phi}$, it reduces to Fowler-Nordheim, or FN-like equation

$$J = \frac{2.2e^3 F^2}{8\pi h \phi_0} \exp\left(-\frac{8\pi}{2.96heF} \sqrt{2m} \cdot \phi_0^{3/2}\right) \quad (3)$$

Tunneling in STM junction may reach this limit under high voltage ($eV \gg \bar{\phi}$) bias. Assuming $F = V/s$, linear relationship of $\ln(I/V^2)$ with (I/V) , called F-N plot, was verified over three orders of magnitude during the preliminary investigations of the STM tunnel junction in high bias regime, as shown in Fig. 6. It has been shown by Saenz and Garcia¹² that STM can be operated in the near-field emission regime without any loss of vertical sensitivity.

3.2 Tip-sample Distance and Image Contrast

Absolute tip-sample distance measurement involves fitting of a theoretical I - s (constant V) curve to the experimental one for a specific sample. In the field emission mode, tip can move to large distance without loss of tunneling current. Exact determination of this allowable tip-sample distance from the I - V data would require knowledge of tip radius and local work function. Under atmospheric conditions, the tip surface composition is ill-defined where many contaminants present can drastically lower the metal work function. Different chemical species present on the sample surface can alter local barrier height, which in turn would affect tunnel current as suggested by Eqn (3) and produce corrugations in STM images to be mistaken as topographical details. This aspect should be kept in mind during imaging with an atmospheric STM. An estimation of tip-sample distance can be made considering that slope of the F-N plot [see Eqn (3)] yields the barrier height as a function of slope of the F-N plot and the tip-sample distance. The slope reduces to

$\approx (he \times slope_{FN} \times s / 12\sqrt{m})^{2/3}$ giving a tip-sample distance of 4 nm to 20 nm corresponding to the barrier height of 1.2 V to 0.5 V respectively. Simmons has shown that image forces of the tunneling electron can suppress the tunneling barrier considerably. Calculations with an experimental set of I - V data on our homebuilt STM in the high voltage regime applied to Simmons' formulation for tunneling current density taking image forces into account¹² gave an estimated lowering by several eV . Contamination under atmospheric conditions also contributes to lowering of the metalwork function. In view of the foregoing, it seems reasonable to believe that the tip-sample distance in this regime should be in excess of 4 nm, which makes it possible to image nanostructures with large roughness levels. It is also interesting to note that since $\phi^{3/2}$ also appears in the negative exponent in the tunneling equation, lowering of the barrier height reduces the overall sensitivity of the tunneling current to the tip-sample distance, making the vibration isolation requirements less stringent.

4. CONCLUSION

The key to advances in nanoscale engineering of materials lies in our ability to synthesise, see, manipulate, replicate, and mass-produce materials that would be the building blocks of novel systems with ultimate miniaturisation. While nanotechnology seems to be a revolution waiting to happen, it is still in its infancy. One is still learning to build and put a few nanoscale pieces together to perform a collective electronic circuit function. A homebuilt LC-STM would prove a convenient tool in preliminary, real-space imaging and tunneling spectroscopy of nanoscale materials paving up the research toward this emerging technology. A detailed account of development of an atmospheric LC-STM has been presented in this paper and low current imaging of a variety of nanoscale samples has been successfully demonstrated. Critical design issues have been elaborated with a view to help researchers from diverse fields to build their own LC-STM at negligible cost.

Though the discussion on its application has been restricted to imaging, the instrument's capabilities

can be substantially enhanced with simple additions. For instance, with a sample-and-hold circuitry combined with voltage ramp, tunneling spectroscopy can be carried out to determine the band structure of nanoscale structures. With these additions, the STM has been successfully used for spectroscopic measurements of capped nanoparticles*. To this end, silver nanoparticles have been prepared using organic molecules of different lengths—ATP (6 Å), PDT (10 Å) and ODT (15 Å) – as capping agents. The single electron tunneling (SET) characteristics of the double-barrier tunnel junctions (DBTJ) formed by these between tungsten tip and gold substrate have also been distinguished. While our experimental results in this direction remain inconclusive for want of theoretical modelling at this stage, the instrument's application to studies of SET effects has been demonstrated.

In this study, the aluminum cover was modified with a hole and rubber isolator to accommodate a photomultiplier tube looking onto the tunnel junction. Attempts to detect photon-emission from rough metallic nanostructures due to inelastic tunneling have also produced encouraging results. A clean (UHV-compatible) heating stage with the temperature range of ambient to 350 °C with accuracy of 0.7 °C has also been developed to study diffusion of nanoparticles under the STM. Temperature stability of several minutes has been achieved by building a constant current power supply for the heater; a simple but effective approach. Humid air was pumped into the chamber (using a small air pump used in household fish pots) to facilitate imaging of biological samples. These are best imaged by LC-STM using the poorly conducting thin aqueous layer under humid conditions. The humidity in the chamber can be monitored using a sensor. It can be seen that there is unlimited scope for investigations using a homebuilt LC-STM since it can be altered to the user's needs.

With these investigations coupled with the growing theoretical understanding of the nano, the nanotechnology could soon attain a level of maturity where it would benefit the defence and space sectors in the visibly near-future. It is hoped that the low cost approach discussed will see a homebuilt STM becoming as much a part of the common materials science laboratory

as the good old optical microscope has been for the routine microscale studies for over a century.

ACKNOWLEDGEMENTS

The study reported here was carried out towards, and subsequent to author's MPhil degree in Department of Physics, University of Pune and at the College of Military Engineering, Pune. Support and facilities provided by Heads of these institutions and Prof C.V. Dharmadhikari during the course of this study are acknowledged. Help of Dr A.O. Ali of Yeman University in initial diagnostic measurements of the tunnel junction is duly acknowledged. CNT sample provided by Dr Kanik Ram of DMSRDE, Kanpur and thiolate and gold-coated Si substrate used for samples depicted in Figs 3 and 8 provided by Dr Sushama Pethkar of NCL are also duly acknowledged.

REFERENCES

1. Balasubramanian, K.; Sordan, R.; Burghard, M. & Kern, K. A selective electrochemical approach to carbon nanotube field-effect transistors. *Nano Letters*, 2004, **4**(5), 827-30.
2. Markovich, G.; Collier, C.P.; Henrichs, S.E.; Remacle, F.; Levine, R.D. & Heath, J.R., Architectonic quantum dot solids. *Acco. Chem. Res.*, 1999, **32**(5), 415-23.
3. Binnig, G. & Rohrer, H. Scanning tunneling microscopy. *IBM J. Res. Develop.*, 1986, **30**(4), 355-69.
4. Wiesendanger, R. Scanning probe microscopy methods and applications. Cambridge University Press, New York, 1994.
5. Tersoff, J. & Hamann, D.R., Theory of the scanning tunneling microscope. *Physical Reviews B*, 1985, **31**(2), 805-13.
6. Yu, E.T. Sectional scanning tunneling microscopy. *Chemical Reviews*, 1997, **97**(4), 1017.
7. Kale, R.K. Feasibility study of low current scanning tunneling microscope, University of Pune, 1998. (MPhil Thesis).

* Kale, R.K.; Pethkar, S.; Vijayamohan, K. & Dharmadhikari, C.V. Role of organic spacers in coulomb blockade of silver nanoparticles. 2003. (Internal report).

8. DiLella, D.P.; Wandass, J.H.; Colton, R.J. & Marrian, C.R.K., Control systems for scanning tunneling microscopes with tub scanners. *Rev. Sci. Instrum.*, 1989, **60**(6), 997-002.
9. Young, R.; Ward, J. & Scire, F. Observation of metal-vacuum-metal tunneling, field emission and the transition region. *Phys. Rev. Lett.*, 1971, **27**, 922-24.
10. Young, R.; Ward, J. & Scire, F. The topographiner: An instrument for measuring surface microtopography. *Rev. Sci. Instrum.*, 1972, **43**, 999-011.
11. Simmons, J.G. Generalised formula for the electric tunnel effect between similar electrodes separated by a thin insulating film. *J. Appl. Phy.*, 1963, **34**(6), 1793-803.
12. Saenz, J.J. & Garcia, R. Near-field emission scanning tunneling microscopy. *Appl. Phys. Lett.*, 1994, **65**(23), 3022-24.

Contributor



Mr R.K. Kale is working as a Scientist in the Dept of Aerospace Engg at the Defence Institute of Advanced Technology (DIAT) (Deemed University), Pune. He is a postgraduate in Physics from Jabalpur University and obtained his MPhil in 1998 from the University of Pune. He joined DRDO in 1983. He served at the Aerial Delivery Research and Development Establishment, Agra, and subsequently at the College of Military Engineering, Pune, before joining DIAT in 2002. Areas of his current interest are missile dynamics, missile system engineering, and nanotechnology.